

# Tracking *C. elegans* Populations in Fluid Environments for the Study of Different Locomotory Behaviors<sup>\*</sup>

G. Tsechpenakis<sup>1</sup>, L. Bianchi<sup>2</sup>, M. Driscoll<sup>3</sup>, D. Metaxas<sup>4</sup>

**Abstract**—We present here a novel automated computer-based approach for analyzing the locomotion of multiple *C. elegans* in low resolution images, based on computer vision methods. With our method, we can provide information on the position of the nematodes, their trajectory and the shape of their body during locomotion. Moreover, our method is designed to efficiently track animals and extract locomotion features in cluttered images and under lighting variations. We use this method to analyze *C. elegans* swimming for the first time in detail and we report features of nematode swimming not previously noted. With our method we were able to distinguish differences between the swimming patterns of different mutants that at first glance appear the same. Finally, in this paper we show numerical results for the swimming patterns of different mutants, and we describe some of our findings.

**Index Terms**—*C. elegans* tracking, locomotion patterns, tracking multiple animals.

## I. INTRODUCTION

**C**AENORHABDITIS *elegans* (*C. elegans*) is a small 1 mm long free-living soil nematode that has been heavily utilized as a model organism to dissect gene function, molecular pathways and genetic influences on behavior. The complete developmental program of cell divisions that make up the 959-celled adult has been cataloged and the connectivity pattern of all 302 neurons has been documented for this transparent animal. The predominant sexual form is hermaphroditic, so that animals can reproduce by self-fertilization. Animals develop from fertilized eggs to reproductive adults in ~3 days, with each capable of producing ~300 genetically identical offspring.

The *C. elegans* lifespan is on the order of ~3 weeks, which has made *C. elegans* a popular organism for analysis of

lifespan genetics. A key experimental advantage is the ease of genetic manipulations that are possible, such that large numbers of mutant strains affecting many aspects of behavior have been isolated. Defining the relationship between gene function and behavior is a major focus in *C. elegans* research. One nematode behavior that can be readily scored and analyzed is locomotion on solid support, such as an agar slab in a lab Petri dish. *C. elegans* moves on its side, with movement forward or backward via an elegant sinusoidal motion that is driven by a series of alternating dorsal-ventral bends. Careful analysis reveals that amplitude of the body bends, time spent in forward and backward movement, and frequency of turns are affected by a plethora of factors including mechanical and chemical stimuli, drugs, temperature, presence of food, and previous experience and age of the animals [2,6,14,24,25]. Thus, analysis of locomotion under different conditions can provide insight into multiple processes. One challenge, however, is that many locomotion parameters are subtle and require video-aided analysis to measure. The reason for that is that the human observer can only provide qualitative or gross description of a motion (e.g., number of animal thrashings, body-bend vs. no bend etc.) and there is always the problem of the human bias.

Some powerful computer-based programs that score *C. elegans* locomotion phenotypes on plates have been developed to facilitate analyses of subtle locomotion phenotypes. One approach published tracks several nematodes simultaneously [5,7,22], which is effective for toxicological and pharmacological assays, but does not report detailed shape-related locomotion features that distinguish animals of different genetic backgrounds or age. An alternative published approach extracts precise shape-related features of single moving nematodes [9,10,11,1,17]. This approach allows classification of nematodes into distinct categories, but can track only one animal at the time and is based on local thresholding. In computer vision, local lighting changes (shadowing effects), low spatial resolution of the images, blurry pixels/regions, etc., can be perceived as noise. The segmentation of the animals using pixel intensity thresholding is usually less robust due to the ambiguities caused by noise.

Computational assistance is less available for other locomotory behaviors in *C. elegans*. The natural *C. elegans* life history in the soil undoubtedly involves encounters with liquid environments, such as introduced by rain. However, very little work has been published on swimming behavior,

<sup>\*</sup>This research was funded by the National Institutes of Health (R21AG027513 and R01AG024882 to M. Driscoll, R21AG027513 to D. Metaxas, and R21NS049511 to L. Bianchi); G. Tsechpenakis and L. Bianchi contributed equally to this work.

<sup>1</sup>Electrical and Computer Engineering Dept., University of Miami. Email: gavriil@miami.edu, tel: (+1)305-284 3340.

<sup>2</sup>Dept. of Physiology and Biophysics, University of Miami. Email: Lbianchi@med.miami.edu, tel: (+1)305-243 1886.

<sup>3</sup>Dept. of Molecular Biology and Biochemistry, Rutgers University. Email: Driscoll@nel-exchange.rutgers.edu, tel: (+1)732-445 7182.

<sup>4</sup>Computer Science Dept., Rutgers University. Email: dnm@cs.rutgers.edu, tel: (+1)732-445 2795.

which is standardly scored by researchers as the rate of body bends per unit time, with one animal scored at a time [21]. Interestingly, rate of body bends/time declines as animals age [13] (our unpublished results), suggesting that analysis of locomotion in liquid media has the potential to aid in the isolation of mutants that age faster or slower than wild type.

Here we document a novel and robust method for fully automated tracking and extraction of locomotion features of multiple *C. elegans* in liquid, based on computer vision techniques. Our method simultaneously tracks many swimming animals that often touch and occlude each other, and extracts both position-related (such as positions and movement paths) and shape-related features (shape deformations and symmetry of deformations). A key advantage of our method is that it can process low resolution images in the presence of noise and local lighting variations. We show that our framework robustly detects differences between mutants that appear similar to human observers and we show how our method can be used to describe and analyze novel locomotion phenotypes. Our framework thus now enables rapid and quantitative scoring of swimming individuals or populations to identify changes induced by genetic, pharmacological, or aging processes.

## II. TRACKING AS A GENERAL PROBLEM

Tracking algorithms can be divided into two general approaches: (i) methods that model backgrounds [12,8,28,27,20], so that the target objects are detected with background subtraction, and (ii) methods that model the foreground (target objects) [16,26,3], i.e., model the movement behavior of the target objects, or use color information of the objects to distinguish them from the background. The former approach requires non-parametric modeling of the background color, grayscale intensity or texture, and robustness depends on how effective this modeling/approximation is. One way to approximate the background color or intensity distribution sufficiently is using a mixture of Gaussians (mixture of parametric distributions) [12,27] or a non-parametric kernel density estimator [8]. An extensive survey on background estimation and a combined method is presented in [28].

Once the foreground and background are separated, the foreground is clustered into groups based on spatial connectivity and/or temporal (motion) continuity criteria. The different approaches that are used to separate (track) different objects can be model-based [18], appearance-based [32], or combinations of model- and appearance-based [31]. Model-based algorithms use a shape/structure model for the target object, allowing the system to search for the transformation that maps the model into the image sequence. Appearance-based methods are based on mapping of the image feature space to the shape configuration space.

Another way to categorize the existing tracking approaches is based on the temporal continuity constraints of the object's motion [31]. In this sense, there are (i) *continuous* (or *temporal*) methods that use both temporal and static information from the input sequence, and (ii) *discrete* (or

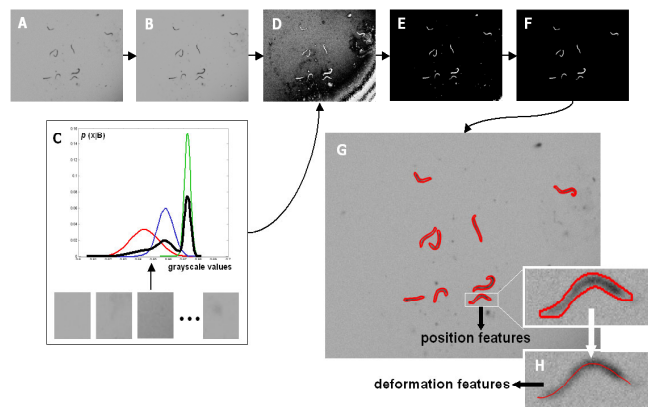


Fig. 1. Our overall framework for simultaneous tracking of multiple nematodes in low resolution for the estimation of position and shape-related locomotion features.

*detection*) methods, which handle each frame separately, using only static information and some kind of prior knowledge (e.g., the shape or motion of the object). Continuous trackers provide high accuracy and low complexity, exploiting the continuity constraints over time, but when programs lose track (e.g., in abrupt or unexpected movements), they usually cannot recover easily; this is a common problem in cases of highly deformable or articulated objects and arbitrary or complex motions. To tackle the problem of the temporal continuity violation in arbitrary and complex motions, the method of S.M. Oh *et al.* [23] was applied to biological studies, and specifically for estimating movement trajectories of animals in dense population environments. This work successfully records the trajectory of multiple animals, e.g. bees, in long duration videos, but it does not handle strongly deformable targets. On the other hand, discrete approaches do not suffer from error accumulation over time, giving independent solutions at each time instance, but their solutions usually do not have temporal coherence, and thus the results have to be registered and filtered [26] over time. Also, this kind of approach often suffers from computational complexity, which is a crucial limiting factor for real-time (>30fps) applications.

## III. TRACKING MULTIPLE *C. ELEGANS*

Our framework for tracking multiple nematodes (*C. elegans*) consists of (i) image pre-processing with Alternating Sequential Filters (ASFs) [19], (ii) probabilistic modeling of the background grayscale intensity, (iii) an appearance-based animal segmentation approach, handling each frame of the sequence independently (detection), and (iv) animal shape registration over time, to establish correspondences between the target animals.

Fig. 1 illustrates the overall framework for the novel vision tracking system we developed. The input image (A) is filtered (B) using an ASF [19] with structuring elements of maximum size 21x21 (for images of 640x480 resolution), and 12 orientations. Then, the probability map (D) is extracted, representing the probability  $P(x|B)$  of the image pixels  $x$  belonging to the background  $B$ . This probability map is estimated using prior knowledge for the background grayscale

distribution (C). Next, the animal region initialization is extracted based on the probability map: (i) the probability of a pixel  $\mathbf{x}_i$  belonging to an animal region  $W$  is calculated as  $P(\mathbf{x}_i|W) = 1 - P(\mathbf{x}_i|B)$ , (ii) a binary animal map (E) is extracted with thresholding the animal probability map (D), (iii) morphological dilation [19] is applied to the binary map to connect pixels that correspond to the same animal but are unconnected, and (iv) the noise (undesired white pixels) of the dilated binary map is eliminated using connectivity and size constraints (F). The resulting regions are used to estimate accurately the animal boundaries (G), using region information and a maximum likelihood approach. The final step of our framework consists of establishing correspondences between successive frames, i.e., registering the animals over time, and estimating the position and deformation parameters from the animal skeletons (H).

### A. Background Modeling

Let  $\Omega$  be the image domain and  $B \subseteq \Omega$  be the background region. To model the background grayscale intensity distribution, we estimate the probability density function  $p_B$  of the intensity values obtained from sample (training) background regions (Fig. 1(C)). Since a single parametric distribution (e.g. Gaussian) cannot sufficiently model the background, we use a mixture of  $n$  Gaussians,

$$p_B = \sum_{i=1}^n \alpha_i \mathcal{G}(\mu_i, \sigma_i^2), \quad (1)$$

where the Gaussian parameters  $(\mu_i, \sigma_i^2)$  and the weights  $\alpha_i$  are estimated by the Expectation Maximization (EM) algorithm [4]. For our application we used  $n = 3$  Gaussians. Fig. 1(C) illustrates the three Gaussians (red, blue, green), and their weighted combination (black) as estimated by the EM algorithm using training background samples.

Then, the probability of a pixel  $\mathbf{x}_i \in \Omega$  with intensity  $I(\mathbf{x}_i)$  being consistent with (belonging to) the background  $B$  is,

$$p(\mathbf{x}_i|B) = \int_{I(\mathbf{x}_i)-dI}^{I(\mathbf{x}_i)+dI} p_B(y) dy, \quad (2)$$

where  $dI$  determines a small grayscale interval.

### B. C. elegans Region Initialization

After extracting the probability map, i.e., the probabilities  $P(\mathbf{x} | B)$  for all pixels  $\mathbf{x} \in \Omega$ , we can estimate the probability of the pixels belonging to the animal regions  $W \subseteq \Omega$  as  $P(\mathbf{x} | W) = 1 - P(\mathbf{x} | B)$ . Fig. 1(D) illustrates an example of the animal probability maps  $P(\mathbf{x} | W)$ . In these images one can see that although most animal pixels are assigned high probabilities (brighter regions), there are some pixels that do not belong to animal regions and are still assigned high probabilities. The reason for this is the undesired dark background regions with grayscale values close to the animal pixels intensities.

Our aim is to obtain sufficient animal region initializations so that we can accurately and efficiently segment the animals from the background. From the animal probability maps  $P(\mathbf{x}|W)$  we can obtain such initializations after eliminating undesired pixels, i.e., pixels that belong to the background but are still assigned high probabilities. For that purpose, we first threshold the animal probability maps with a high value (close to 1), as shown in Fig. 1(E). In this step we exclude (from the initializations) regions that have lower probabilities. Note that

sufficient background modeling, i.e., using sufficient knowledge for the background intensity distribution, results in smaller and fewer background regions with high values of  $P(\mathbf{x}|W)$ .

In order to exclude isolated pixels or small groups of pixels with probabilities higher than the threshold, we apply size and pixel connectivity constraints to the dilated binary image (thresholded animal probability map): isolated pixels are excluded as noise, and small groups of pixels are excluded if their size (number of pixels) is smaller than the expected animal size (area). Fig. 1(F) illustrates the obtained animal region initializations following the steps described above.

Obviously, compared to a simple (deterministic) intensity thresholding, the above probabilistic approach provides better and more robust animal-region initializations under lighting variations and noise.

### C. C. elegans Shape Estimation

In [29,30], we have showed how accurate object segmentation can be achieved in cases of insufficient boundary information, similar to the low resolution animal regions. Due to the computational complexity of these methods though, we follow here another approach. Once the animal regions are initialized, we estimate each animal's shape based on the local region information, in an iterative manner, as follows.

We design a Maximum Likelihood (ML) intensity term that forces the animal initialization toward areas where the pixel probabilities of belonging to the animal interior ( $W$ ) are high. This ML term is formalized by maximizing the log-likelihood of pixel intensities in a narrow band around an estimated animal boundary after every iteration.

More specifically, let  $\mathbf{C}_0^t$  be the animal initialization at time  $t$ . The final animal shape  $\mathbf{C}^t$  is obtained by maximizing the log-likelihood of the pixel intensities in the interior of the curve. Thus, the final animal shape at time  $t$  is estimated as,

$$\mathbf{C}^t = \arg \max \iint_{R_C} \log P(\mathbf{x}|W) d\mathbf{x}, \quad (3)$$

where  $R_C$  is the image region enclosed by the evolving boundary  $\mathbf{C}^t$  at time  $t$ .

Note that using this log likelihood in the above equation, we assume that the pixel sites are statistically independent. In contrast to our previous work of [29,30], we make this assumption to avoid the computational cost of a probability propagation over neighboring pixels similar to e.g. the Conditional Random Fields used in [29,30], or the common Markov Random Fields. In our application this simplifying assumption gives us good boundary results with time efficiency.

After obtaining the animal boundary, we smooth it with a Gaussian kernel. Fig. 1(G) illustrates the result of the boundary estimation for all the animals of the image.

Fig. 2 illustrates another, more detailed, example of the animal shape estimation based on the above ML approach: the two rows correspond to different animal instances; the first column illustrates the filtered grayscale regions of the images, the second column shows the animal boundaries initialization;

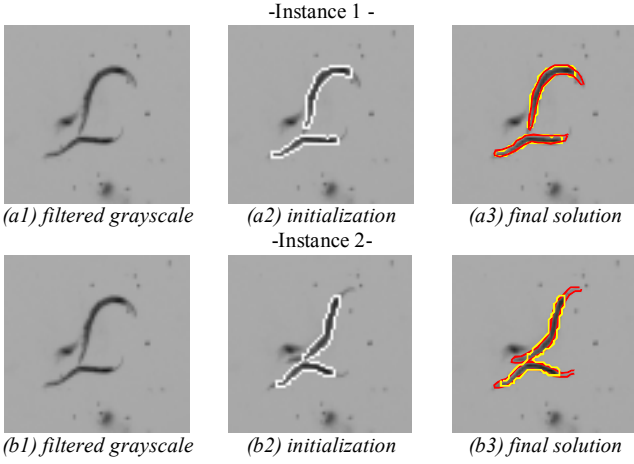


Fig. 2. An example of the animal shape estimation based on our Maximum Likelihood approach using the animal initializations.

in the third column, the animal initial boundaries are shown in yellow lines, and the final solution of eq.(3) is shown in red lines. Note that when two animals touch or occlude each other (second row), we first detect the intersection point(s) and then we split the extracted boundary into two curves.

#### D. *C. elegans* Temporal Registration

When there is more than one target animal, we need to register the extracted shapes, i.e., establish correspondences between the animals over time, so that for each animal we can obtain motion information for the entire sequence.

Shape registration is critical to various computer vision and medical imaging applications [33]. Global registration, also known as shape alignment, aims to recover a global transformation that brings the pose of a source shape as close as possible to that of a target shape. Moreover, to account for local deformations, non-rigid local registration [15] is needed to establish dense correspondences between the basic elements of shapes, such as points, curvature, etc.

In our framework, we adopt a simple distance measure approach for animal registration. Let  $\mathcal{C}^t$  be the set of all animal shapes  $\mathbf{C}_i^t$  estimated at time  $t$ , with  $i = 1, \dots, N_t$ , and  $N_t$  denoting the total number of animals detected at time  $t$ . Also, let  $\mathcal{C}^{t+1}$  be the set of animal shapes  $\mathbf{C}_j^{t+1}$  estimated at time  $t+1$ , where  $j = 1, \dots, N_{t+1}$ , and  $N_{t+1}$  is the number of animals detected at time  $t+1$ ; note that it is not necessarily  $N_t = N_{t+1}$  (same number of detected animals in both frames). If  $\mathbf{R}_i^t$  and  $\mathbf{R}_j^{t+1}$  are the regions enclosed by the boundaries  $\mathbf{C}_i^t$  and  $\mathbf{C}_j^{t+1}$  respectively, then for each animal shape  $\mathbf{C}_i^t \in \mathcal{C}^t$  we search for the estimated shape  $\mathbf{C}_k^{t+1} \in \mathcal{C}^{t+1}$  that minimizes a distance between the regions  $\mathbf{R}_i^t$  and  $\mathbf{R}_k^{t+1}$ . To measure the above distance, we use the chamfer distance which is defined as follows.

In general, given two point sets  $A$  and  $B$ , their undirected chamfer distance  $d(A, B)$  is defined by the forward and backward distances  $d^f(A, B) = \frac{1}{\|A\|} \sum_{a^i \in A} \min_{b^j \in B} \|a^i - b^j\|$  and  $d^b(A, B) = \frac{1}{\|B\|} \sum_{b^j \in B} \min_{a^i \in A} \|a^i - b^j\|$ , respectively, as

$$d(A, B) = d^f(A, B) + d^b(A, B) \quad (4)$$

According to the above, we search for the  $k$ -th estimated animal shape at time  $t+1$ , belonging the set of all shapes  $\mathcal{C}^{t+1}$  that minimizes the chamfer distance  $d(\mathbf{R}_k^{t+1}, \mathbf{R}_i^t)$  between its enclosed region  $\mathbf{R}_k^{t+1}$  and the estimated region  $\mathbf{R}_i^t$  at time  $t$ . Thus, the  $k$ -th estimated shape at time  $t+1$  is assigned to the  $i$ -th animal at time  $t$  as,

$$k = \arg \min_{k \in \{1, \dots, N_{t+1}\}} d(\mathbf{R}_k^{t+1}, \mathbf{R}_i^t) \quad (5)$$

The distance  $d(\cdot, \cdot)$  is calculated based on eq.(4), replacing  $A$  and  $B$  with the regions (pixel sets)  $\mathbf{R}_k^{t+1}$  and  $\mathbf{R}_i^t$ , respectively. Also, note that this distance can be used for point sets of different sizes, and therefore we can use it as a general similarity measure.

Fig. 3 illustrates our tracking results in three nearly successive frames of a sequence: the red lines represent the extracted animal skeletons superimposed on the original grayscale images.

#### IV. C. ELEGANS LOCOMOTION FEATURES

Using the tracking results of our method, we can estimate a number of locomotion features to describe the *C. elegans* movement. These features were chosen as a good approximation of what the experts have been “manually” observing with the microscope so far.

We estimate two categories of locomotion features: (i) *position-related* features, that are estimated from the position of the animals on the image plane over time, and (ii) *shape-related* features, that refer to the shape of the extracted animals over time. An important property of our framework is that it can be adapted to user needs: since tracking provides accurately both shape and position for all animals, we are able to estimate any potential locomotion features defined by the researcher.

##### A. Position-related Locomotion Features

These features can be extracted by tracking the center of mass of each animal over time, and they do not include shape information. In the following we describe the features belonging to this category, namely (i) the position, (ii) the translation, (iii) the percentage of animals moving per unit of time (movement percentage).

**Position.** Let  $\mathcal{M}_i^t(\mathbf{t}) \in \mathbf{R}_i^t$  be the center of mass of the  $i$ -th target animal on the image plane, at time  $t$ , where  $\mathbf{R}_i^t$  is the region enclosed by the estimated animal boundary.  $\mathcal{M}_i^t(\mathbf{t})$  can be calculated as,

$$\mathcal{M}_i^t(\mathbf{t}) = \frac{1}{\mathcal{A}_i} \sum_{k=1}^{\mathcal{A}_i} \mathbf{x}_k(\mathbf{t}), \quad (6)$$

where  $\mathcal{A}_i$  is the number of pixels within the animal region  $\mathbf{R}_i^t$ , and  $\mathbf{x}_k(\mathbf{t}) \in \mathbf{R}_i^t$  are the animal pixel coordinates on the image plane at time  $t$ .

**Translation.** From the definition above, the translation  $\mathcal{V}_i^t$  of the  $i$ -th animal at time  $t$ , is calculated as the change of the position between times  $t-1$  and  $t$ , i.e., the first derivative of the position of the animal center of mass,

$$\mathcal{V}_i^t = \left. \frac{\partial \mathcal{M}_i}{\partial \mathbf{t}} \right|_{\mathbf{t}} \cong \|\mathcal{M}_i(\mathbf{t}) - \mathcal{M}_i(\mathbf{t} - 1)\| \quad (7)$$

**Movement percentage.** If  $N_t$  is the number of animals detected in the examined field (image plane), then it is

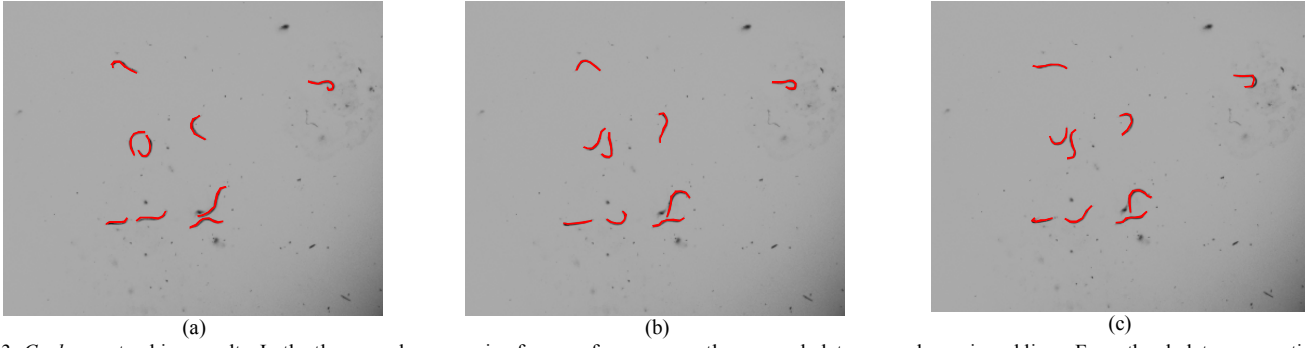


Fig. 3. *C. elegans* tracking results. In the three nearly successive frames of a sequence, the worm skeletons are shown in red lines. From the skeletons we estimate the shape and position-related locomotion features of the animals per frame and over time.

straightforward to estimate the ratio of the moving animals vs. the entire detected animal population  $N_t$ , per frame. For the estimation of this ratio, motion is calculated from eq.(7) and immobility is detected when the translation is lower than a pre-defined threshold. This ratio, estimated for all frames of a sequence, gives as an overall observation of the moving ability of an animal population.

Note that the above locomotion features do not “carry” any shape information for one main reason: to describe the nature of the translational movement and the deformations separately. For example, when the center of mass of a nematode remains at the same position on the plate over some time, while its body is deforming, this is also important information: that shows that the locomotion of the worm is strongly deformable and not translational (it does not “travel” much on the plate).

### B. Shape-related Locomotion Features

While the position-related locomotion features described above can give us information about the movement path (trajectory) of each animal of the examined population, they do not provide us local shape-related information. Therefore, to take into account animal shapes and shape changes over time, we estimate features that we define as shape-related, since they describe locally the animal deformations. In the following we describe these shape-related features, namely (i) the motion, (ii) the inter-frame deformation, (iii) the absolute deformation, (iv) the deformation symmetry, and (v) the shape frequencies.

To estimate some of the shape-related locomotion features, and for complexity reduction purposes, instead of using the extracted sets of animal regions  $\mathcal{R}^t$ , or boundaries (contours)  $\mathcal{C}^t$ , at every time  $t$ , we use skeletons of the animal regions.

For a detected animal at time  $t$ , its skeleton is defined as the open 1D curve  $\mathcal{S}^t$  that preserves the animal’s region topology, extent and connectivity:  $\mathcal{S}^t = [\mathbf{x}_s^t(k) \mid k = 1, \dots, n]$ ,  $\mathbf{x}_s^t(k)$  are the Cartesian coordinates of each skeleton point, and  $n$  is the total number of skeleton points.

**Worm motion.** Let  $\mathcal{S}^{t-1}, \mathcal{S}^t$  be the skeletons of a animal extracted at times  $t-1$  and  $t$ , respectively. Then, the motion  $m^t$  of the animal between these two time instances is defined in terms of the undirected chamfer distance of eq.(4):

$$m^t = d(\mathcal{S}^{t-1}, \mathcal{S}^t) \quad (8)$$

The above notion does not allow for discrimination between deformation and translation and it gives us the animal displacement due to both kinds of movement.

**Inter-frame deformation.** Another potentially useful measurement is the pure animal deformation over time, excluding the translation effect. In order to estimate these deformations, we need to describe the animal shape changes independently from any translation, using a translation-invariant quantity. Therefore, we use the skeleton’s curvature function defined below.

Let  $\mathbf{x}_s^t(k) = [x_s^t(k), y_s^t(k)]$ , with  $k=1, \dots, n$ , be the Cartesian coordinates of an animal skeleton. Then, the curvature function is defined analytically as,

$$\mathcal{C}^t = \frac{x_s^t(k) y_s^t(k) - x_s^t(k) y_s^t(k)}{\{[x_s^t(k)]^2 + [y_s^t(k)]^2\}^{3/2}} \quad (9)$$

where  $\dot{x}_s^t(k)$ ,  $\dot{y}_s^t(k)$  and  $x_s^t(k)$ ,  $y_s^t(k)$  are the first and second derivatives at a curve location  $k$  respectively. These derivatives are approximated using (finite) centered differences between successive skeleton points.

Thus, given the skeleton curves  $\mathcal{S}^{t-1}, \mathcal{S}^t$  and their corresponding curvature functions  $\mathcal{C}^{t-1}, \mathcal{C}^t$  as defined above, the animal deformation is calculated as the chamfer distance,

$$m_D^t = d(\mathcal{C}^{t-1}, \mathcal{C}^t) \quad (10)$$

**Absolute deformation.** In a similar way to estimating the animal deformation over time (inter-frame), we estimate the *absolute* deformation, i.e., the variation of the animal shape (skeleton curve) from the straight line connecting the two ends (head and tail) of the skeleton. This measurement can be also seen as the *quality* or *magnitude* of deformation.

Thus, if  $\mathcal{S}^t$  is the skeleton curve at time  $t$ , and  $\mathcal{L}^t$  is the straight line connecting the two ends of the animal, the absolute deformation is defined as the chamfer distance,

$$m_A^t = d(\mathcal{S}^t, \mathcal{L}^t) \quad (11)$$

**Deformation symmetry.** We estimate the symmetry of an animal shape at time  $t$ , based on its skeleton symmetry with respect to the animal center  $\mathcal{M}(t)$  and the straight line  $\mathcal{L}^t$  connecting the two ends of the skeleton curve. Let  $\mathcal{S}^t$  be the skeleton curve function aligned according to the rotation angle  $a$  between the line  $\mathcal{L}^t$  and the horizontal ( $x$ -) axis (Fig. 4(a)). Then, if  $xy'$  is the coordinate system centered at  $\mathcal{M}(t)$ , such that  $\mathcal{S}^t(x) = y'$ , a symmetric animal shape would correspond

to an even or odd function  $\mathcal{S}^t$  with respect to the new coordinate system, i.e.,  $\mathcal{S}^t(x) = \mathcal{S}^t(-x)$  or  $\mathcal{S}^t(x) = -\mathcal{S}^t(-x)$  respectively. The first condition indicates that the function  $\mathcal{S}^t$  is symmetric around the  $y'$  axis, whereas the second condition indicates symmetry around the center  $\mathcal{M}^t$ . Thus, we define as *symmetry error*,

$$\mathcal{E}_{\text{sym}} = \sum_{k=1}^{n^t/2} \|\mathcal{S}^t(k) - \mathcal{S}^t(-k)\|, \quad (12)$$

where  $n^t$  is the animal (skeleton) length at time  $t$ . If the skeleton  $\mathcal{S}^t$  is symmetric either around the center of mass or the  $y'$  axis, then  $\mathcal{E}_{\text{sym}} = 0$ ; obviously, the less symmetric the skeleton is, the higher the symmetry error is.

**Shape frequencies.** In our framework we determine as shapes of interest body shapes similar to the letters 'C', 'I', 'S' and 'O', respectively; therefore, we will refer to this feature as *CISO* descriptor, which is a 4x1 vector containing these frequencies. Let  $\text{letter} = \{C, I, S, O\}$  be the vector containing the number of times that each shape label appears in the video of  $T$  frames, for a specific animal. Then the *CISO* descriptor is  $\mathcal{F}_{\text{CISO}} = \frac{\text{letter}}{T}$ .

In order to determine when an animal body forms one of the above shapes of interest, we first need to have a detailed shape description. For that purpose, we use the shape histogram described below.

To describe the shape of a animal, we use the 2D shape histogram  $h_i^t(r, \varphi)$  that represents the distribution of the skeleton points of the  $i$ -th animal, at time  $t$ , according to the (radial) distance  $r$  from the animal center  $\mathcal{M}_i^t$  and the angle  $\varphi$  (Fig. 4(b)). Thus, each bin of the shape histogram represents the percentage of the animal points within the image region defined by  $dr$  and  $d\varphi$ ,

$$h_i^t(dr, d\varphi) = \frac{1}{n_i^t} \sum_{dr} \sum_{d\varphi} \mathcal{S}_i^t(k, l) dk dl, \quad (13)$$

where  $n_i^t$  is the animal (skeleton) length at time  $t$  and  $\mathcal{S}_i^t(k, l)$  is the skeleton part within the image region defined by the radial distance  $k$  and the angle  $l$ . Using the shape histogram of eq.(13) we are able to recognize, at each frame, which shape of interest (*CISO*) each target animal forms, as follows.

Similarly to the background modeling (training phase) described in III(A), we model each one of the shapes of interest off-line. For that purpose, and for each shape of interest, we estimate the histograms of sample animals when they form the specific shape. Then we calculate the mean histogram, i.e., a histogram each bin of which corresponds to the mean value of the respective bins of the estimated histograms,

$$\bar{h}_l^t(dr, d\varphi) = \frac{1}{\mathfrak{N}} \sum_{k=1}^{\mathfrak{N}} h_k^t(dr, d\varphi), \quad (14)$$

where  $\mathfrak{N}$  is the number of histograms estimated from the sample animal skeletons,  $l$  is the index for one of the four shapes (letters) of interest (*CISO*), and  $h_k^t(dr, d\varphi)$  is the bin defined by  $(dr, d\varphi)$  of the  $k$ -th histogram estimated for the shape of interest  $l$ . After estimating a mean shape histogram for each shape of interest, we recognize (label) the input animal shapes according to histogram distances.

Let again  $h_i^t(r, \varphi)$  be the shape histogram of the  $i$ -th animal estimated at time  $t$ . Also, let  $\bar{h}_l^t(r, \varphi)$  be the mean histogram

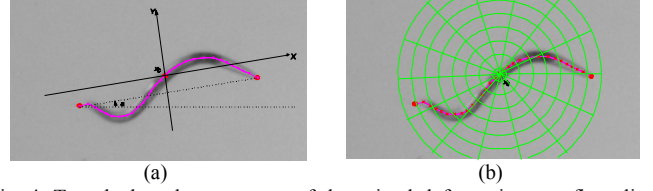


Fig. 4. To calculate the symmetry of the animal deformation, we first align the skeleton shown in pink (a), using the straight line connecting the two ends of the animal (red dots). In the new (rotated) coordinate system defined by this line and the axis normal to it, we use the skeleton as a function to determine whether it is even (symmetric to the new vertical axis) or odd (symmetric to the system center). To describe the shape of the animal (b), we use the 2Dshape histogram: this represents the distribution of the skeleton points (red dots) according to (i) the (radial) distance from the animal center and (ii) the orientation angle on the image plane, with respect to the skeleton center and the horizontal axis. The bins of the shape histogram represent the percentages of the animal points within the image regions (radial green grid) defined by the radial distances and the orientation angles.

estimated off-line for each one of the labels  $l = \{C, I, S, O\}$ . Then, we calculate the histogram intersection in its Minkowski distance form,

$$D_k(h_i^t, \bar{h}_l^t) = 1 - \sum_{p=0}^{\mathfrak{N}} \sum_{q=0}^{2\pi} \|h_i^t(p, q) - \bar{h}_l^t(p, q)\|, \quad (15)$$

where  $\mathfrak{N} \in \mathbb{N}^+$  is the radial distance constrained by the image domain. Thus, for each target animal we estimate the four histogram intersections of eq.(15), and the  $i$ -th animal shape at time  $t$  is labeled as,

$$l_i^t = \arg \max_l D_k(h_i^t, \bar{h}_l^t), \quad (16)$$

i.e., the animal is assigned the label  $l$  that maximizes the corresponding histogram similarity.

Note that when comparing two skeletons of different scales, the radial distance boundary  $\mathfrak{N}$  varies and thus the two shapes need to be aligned. In our case, we compare shapes of the same scale (resolution) and thus no alignment is needed.

## V. EXPERIMENTAL RESULTS

### A. Manual Scoring versus Computer-aided Analysis

*C. elegans* swimming vigor is often used by researchers as a measure of neuronal and muscular function in mutant strains and to study age decline. Typically, one animal at the time is placed in a liquid media and number of body bends per minute is scored [13, 21]. Gross defects are identified in this manner as reduced number of body bends per minute. More subtle defects, however, escape this type of analysis. In fact, beside the number of body bends per minute, *C. elegans* locomotion in liquid, is not a well-characterized behavior in the lab. We expected that our motion analysis program should accurately describe wild type swimming and robustly report differences in swimming profiles of mutants that exhibit subtle changes that are normally challenging for a human observer to score.

To test this hypothesis, we analyzed swimming behavior of wild type and several allelic variants of *unc-8* (uncoordinated). *unc-8* encodes a DEG/ENaC ion channel subunit expressed in many neurons, including interneurons and motoneurons required for locomotion on a solid surface. *unc-8* gain-of-function mutation *n491* induces neuronal dysfunction and confers a nearly paralyzed coiled phenotype. Intragenic *unc-8*

second-site loss-of-function mutations isolated from this paralyzed strain are thought to be potential *unc-8* null mutations that should "revert" the severely uncoordinated phenotype, restoring near normal locomotion on plates. We also tested a null allele of DEG/ENaC *mec-4*, which is expressed in, and required for the function of, gentle touch sensory neurons. *mec-4* mutants appear lethargic in locomotion on solid support. We also tested an allele of *odr-1*, which encodes a putative guanylyl cyclase expressed in chemosensory neurons and required for normal responses to volatile odorants sensed by neuron AWC, but is not known to impact locomotion.

In a first test of our swimming analysis program, we compared manual scoring of body bend frequency during swimming (body bends counted for 30 seconds) to that reported by our computer vision program for wild type and the *unc-8(n491n1193)* mutant strain. We document wild type to accomplish 43.9 bb/30 sec, a number in good agreement with automated scoring (46.2 bb/30 sec). Similarly our manual counting of *unc-8 (n491n1193)* body bends matches the automated scoring (13.3 versus 13.7 bb/30 sec for manual and automated scoring respectively). Importantly, our analysis confirms that the computer swimming analysis program provides an accurate evaluation of the readily scored parameter of body-bend frequency, validating its use in quantitation of swimming behavior.

We then proceeded to manually count body bends for the other seven mutants (Fig. 5). We found that most second-site *unc-8* mutants did swim with an increased rate of body bends relative to the *unc-8(n491)* mutants. However, we noticed that in some mutants swimming was performed at reduced extent of body bending, a parameter that we could not efficiently score manually.

### B. Automatic Tracking and Feature Extraction

To overcome the problems of quantification of subtle changes and subjectivity in scoring, we used our methods for automatic tracking of nematodes and extraction of both position-related (such as positions and movement paths) and shape-related features (magnitude of inter-frame deformations, shapes, normal and directional speeds, symmetry of deformations) to compare swimming profiles of wild type and selected mutants. Fig. 6 shows the results for the average motion in each frame. Similar differences between wild type and mutants were revealed by our analysis of distance covered per frame and absolute deformation (not shown).

Results are striking in that they clearly underscore that the *unc-8* revertant loss-of-function mutants have swimming performance distinct from wild type (although they are not as impaired as the severely uncoordinated mutants), even though frequency of body bends for some mutants is greater in mutants than wild type. Our analysis clearly demonstrates that our method can detect and quantitatively score defects in the swimming patterns such as shallower body bends that are challenging for human investigators to record. Using our system, we also calculated the percentage of animals moving in each frame. We found that, results matched exactly data

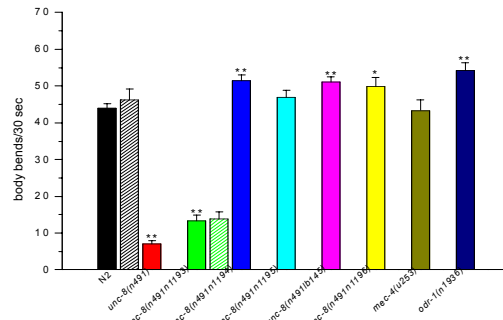


Fig. 5. Body bend frequency for swimming WT and mutant L4 nematodes as determined by manual counting (solid bars) and by the use of our program (shaded bars). We manually scored the number of body bends beginning one minute after individual animals were transferred into 50  $\mu$ l of M9 buffer, room temperature. Each bar represents the average from 30 individually scored animals. For scoring of body bends using our automated approach, we used the thresholded difference between the maximum and minimum absolute deformation of the animals within 1sec time-frame;  $p < 0.05$ ; \*\*  $p < 0.01$  by comparison with wild type, by t Test. Data are expressed as mean  $\pm$  SE.

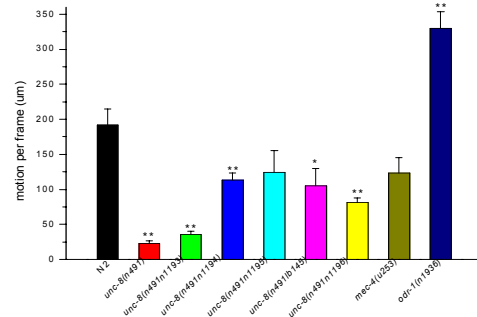


Fig. 6. Comparison of motion per frame in wild type and mutant L4 nematodes.

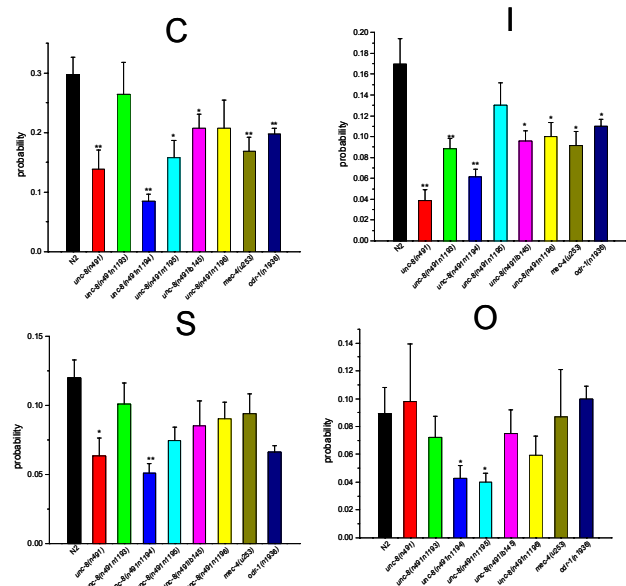


Fig. 7. Comparison of body shape profiles of wild type and mutants. We extracted the frequency of occurrence of body shapes resembling C, I, S, and O as described in Fig. 5. Note that most mutants show a decrease in frequency of at least 2 body shapes, suggesting that their bodies move in a more disordered fashion during swimming. We interpret this as an indication of uncoordinated movement in liquid medium. Number of videos used for each genotype was 5 to 10 (25 to 100 animals). \*  $p < 0.05$ ; \*\*  $p < 0.01$  by comparison with wild type, by t Test. Data are expressed as mean  $\pm$  SE.

shown in Fig. 5 underscoring that if the only parameter that is scored (by human observers or by computer program) is movement versus no movement, only the severely impaired mutants (*unc-8(n491)* and *unc-8(n491n1193)*) stand out as poor swimmers (not shown).

We also classified body shapes into four categories based on the resemblance to letters C, I, S, O, and found that all mutants tested displayed reduction in frequency of the all body shapes (Fig. 7). We interpret the combined reduction of frequency of C, I, S, O shapes to reflect an increase in the frequency of less orderly body shapes. Interestingly, all strains tested display the same rate of symmetry for the anterior and posterior body regions during swimming and the same inter-frame deformation, suggesting that physical and/or anatomical constraints may impose limitations on how these parameters change in swimming *C. elegans*.

## VI. CONCLUSIONS

We presented an automated method that provides a detailed description of multiple *C. elegans* swimming. Our method combines the advantages of previously reported tracking methods for locomotion that either (i) extract both shape and position-related features but can only score individual animals, or (ii) track multiple animals simultaneously, but extract only position-related features. Our method significantly changes the resolution at which we can dissect roles of cells and genes on swimming behavior. In addition, this automated analysis could extend the resolution of drug testing. Another potentially very powerful application should be characterization of age-related locomotion decline. Definition of aging profiles will enable high throughput screens for genetic or pharmacological interventions that promote healthspan and delay locomotory aging. Our computational framework can be generalized to include animal crawling, extending the number of applications for which our approach can be used.

## REFERENCES

- [1] J.-H. Baek, P. Cosman, Z. Feng, J. Silver, and W. R. Schafer, 'Using machine vision to analyze and classify *Caenorhabditis elegans* behavioral phenotypes quantitatively,' *Journal of Neuroscience Methods*, 118:9-21, 2002.
- [2] C. I. Bargmann, 'Genetic and cellular analysis of behavior in *C. elegans*,' *Annu Rev Neurosci*, 16:47-71, 1993.
- [3] D. Comaniciu, V. Ramesh, and P. Meer, 'Kernel-based object tracking,' *IEEE Trans. on Pattern Analysis and Machine Intelligence*, 25(5), May 2003.
- [4] F. Dellaert, 'The Expectation Maximization Algorithm,' *Technical Report GIT-GVU-02-20, College of Computing, Georgia Institute of Technology*, 2002.
- [5] M. de Bono, and C. I. Bargmann, 'Natural variation in a neuropeptide y receptor homolog modifies social behavior and food response in *C. elegans*,' *Cell*, 94:679-689, 1998.
- [6] M. de Bono, and A. V. Maricq, 'Neuronal substrates of complex behaviors in *C. elegans*,' *Annu Rev Neurosci*, 28:451-501, 2005.
- [7] R. Dhawan, D. B. Dusenbery, and P. L. Williams, 'Comparison of lethality, reproduction, and behavior as toxicological endpoints in the nematode *Caenorhabditis elegans*,' *J. Toxicol. Environ. Health*, 58:451-462, 1999.
- [8] A. Elgammal, R. Duraiswami, D. Harwood, L.S. Davis, 'Background and foreground modeling using non-parametric kernel density estimation for visual surveillance,' *Proc. of The IEEE*, Vol. 90, 1151-1163, 2002.
- [9] W. Geng, P. Cosman, C. C. Berry, Z. Feng, and W. R. Schafer, 'Automatic Tracking, Feature Extraction and Classification of *C. elegans* Phenotypes,' *IEEE Trans. on Biomedical Engineering*, 51(10), Oct. 2004.
- [10] W. Geng, P. Cosman, J.-H. Baek, C. Berry, and W. R. Schafer, 'Image Feature Extraction and Natural Clustering of Worm Body Shapes and Motion Characteristics,' *IASTED Int'l Conf. on Signal and Image Processing (SIP 2003)*, Hawaii, Aug. 2003.
- [11] W. Geng, P. Cosman, J. H. Baek, C. C. Berry, and W. R. Schafer, 'Quantitative classification and natural clustering of *Caenorhabditis elegans* behavioral phenotypes,' *Genetics*, 165:1117-1126, 2003.
- [12] M. Harville, G. Gordon, J. Woodfill, 'Foreground Segmentation using Adaptive Mixture Models in Color and Depth,' *IEEE Workshop on Detection and Recognition of Events in Video*, July 2001.
- [13] M. Hertweck and R. Baumeister 'Automated assays to study longevity in *C. elegans*,' *Mech Ageing Dev.* 126(1):139-45, 2005.
- [14] O. Hobert, 'Behavioral plasticity in *C. elegans*: paradigms, circuits, genes,' *J Neurobiol*, 54:203-223, 2003.
- [15] X. Huang, N. Paragios, and D. Metaxas, 'Shape Registration in Implicit Spaces using Information Theory and Free Form Deformations,' *IEEE Trans. Pattern Analysis and Machine Intelligence*, 28(8):1303-1318, Aug. 2006.
- [16] M. Isard, and A. Blake, 'CONDENSATION - Conditional Density Propagation for Visual Tracking,' *International Journal on Computer Vision*, 29(1), 1998.
- [17] W. Li, Z. Feng, P. W. Sternberg, and X. Z. S. Xu, 'A *C. elegans* stretch receptor neuron revealed by a mechanosensitive TRP channel homologue,' *Nature*, 440:684-687, 2006.
- [18] S. Lu, D. Metaxas, D. Samaras and J. Oliensis, 'Using Multiple Cues for Hand Tracking and Model Refinement,' *IEEE Conf. on Computer Vision and Pattern Recognition*, 2003.
- [19] P. Maragos, 'Noise Suppression,' *The Digital Signal Processing Handbook*, V.K Madisetti and D.B Williams Eds., CRC Press, 1998, Chapt. 74, pp. 20-26.
- [20] S. McKenna, Y. Raja, and S. Gong, 'Tracking color objects using adaptive mixture models,' *Image and Vision Computing Journal*, 17:223-229, 1999.
- [21] K. G. Miller, M. Nguyen, A. Alfonso, J. A. Crowell, C. D. Johnson, and J. B. Rand, 'A genetic selection for *Caenorhabditis elegans* synaptic transmission mutants,' *PNAS*, 93:12593-8, 1996.
- [22] Noldus Information Technology®, EthoVision®, <http://www.noldus.com/site/doc/200403002>.
- [23] S.M. Oh, J.M. Rehg, and F. Dellaert, "Parameterized duration modeling for switching linear dynamic systems," *IEEE International Conference on Computer Vision and Pattern Recognition (CVPR'06)*, NYC, June 2006.
- [24] J. T. Pierce-Shimomura, T. M. Morse, and S. R. Lockery, 'The fundamental role of pirouettes in *Caenorhabditis elegans* chemotaxis,' *J Neurosci*, 19:9557-9569, 1999.
- [25] W. R. Schafer, 'Deciphering the neural and molecular mechanisms of *C. elegans* behavior,' *Curr Biol*, 15: 723-729, 2005.
- [26] H. Sorenson, 'Kalman Filtering: Theory and Application,' IEEE Press, 1985.
- [27] C. Stauffer and W.E.L. Grimson, 'Adaptive background mixture models for real-time tracking,' *IEEE Conf. on Computer Vision and Pattern Recognition*, 1999.
- [28] K. Toyama, J. Krumm, B. Brumitt, B. Meyers (1999). Wallflower: Principles and Practice of Background Maintenance. ICCV 1999. pp 255-261.
- [29] G. Tsechpenakis, and J. Wang, "CRF-based Segmentation of Human Tear Meniscus Obtained with Optical Coherence Tomography," *IEEE International Conference on Image Processing (ICIP'07)*, San Antonio, TX, September 2007.
- [30] G. Tsechpenakis, and D. Metaxas, "CRF-driven Implicit Deformable Model," *IEEE Conference on Computer Vision and Pattern Recognition (CVPR'07)*, Minneapolis, MN, June 2007.
- [31] G. Tsechpenakis, D. Metaxas, and C. Neidle, 'Learning-based Coupling of Discrete and Continuous Trackers,' *Computer Vision and Image Understanding*, Oct. 2006.
- [32] G. Tsechpenakis, K. Rapantzikos, N. Tsapatsoulis and S. Kollias, 'A Snake Model for Object Tracking in Natural Sequences,' *Elsevier, Signal Processing: Image Communication*, 19(3):219-238, 2004.
- [33] R. Veltkamp and M. Hagedoorn, 'State-of-the-art in Shape Matching,' Tech. Rep. UU-CS-1999-27, Utrecht University, 1999.